Effect of Reagent Vibration on the H + HOD Reaction: An Example of Bond-Specific Chemistry

Michael J. Bronikowski,† William R. Simpson, and Richard N. Zare*

Department of Chemistry, Stanford University, Stanford, California 94305

Received: August 4, 1992; In Final Form: October 1, 1992

OH and OD product branching ratios and internal state distributions have been measured in a state-to-state study of the reaction $H + HOD(v_1,v_2,v_3) \rightarrow OH(v,N)(OD(v,N)) + HD(H_2)$. The HOD molecules are prepared in a specific vibrational level (one or two J states) by infrared excitation of thermal HOD using a tunable optical parametric oscillator. Fast ("hot") H atoms are generated by laser photolysis of HI at 266 nm, and the OH and OD reaction products are probed quantum-state-specifically by laser-induced fluorescence. The OD:OH product branching ratios demonstrate that we achieve bond-specific chemistry at the lowest possible level of vibrational excitation for the H + HOD reaction: excitation of either bond with one quantum of vibration leads to selective cleavage of that bond. The OD:OH ratio is 1.38 ± 0.14 for the reaction H + HOD(0,0,0) (ground-state HOD). In contrast, this ratio is greater than 25:1 for H + HOD(0,0,1) and less than 1:5.8 for H + HOD(1,0,0) (i.e., OH:OD > 5.8:1). Here (0,0,1) and (1,0,0) denote the O–H and O–D stretch fundamentals, respectively. We find that excitation of these stretching vibrations increases the reaction cross section by a factor of as much as 120 over the increase resulting from an equivalent amount of extra translational energy, which is the behavior expected for a reaction with a late barrier. These results can also be understood in terms of a simple geometric model of the reaction, wherein vibrational excitation widens the cone of acceptance for reaction. The reaction H + HOD(1,0,0) produces a small amount of OD(v=1), which is approximately 5% of the amount of OH(v=0) produced. No vibrationally excited OH or OD was observed in the reactions with HOD(0,0,1) or HOD(0,0,0). OH and OD product rotational and electronic fine-structure distributions were also measured, as were the product state distributions for the reactions H + H_2O and H + D_2O (for comparison to the title reaction). All rotational distributions are well described by temperatures (i.e., Boltzmann distributions); OD products are consistently hotter than OH products (930 K vs 660 K). This observation suggests that rotational excitation of the hydroxyl product occurs mainly through impulsive energy release in the breaking of the OH or OD bond. The $\Pi(A')/\Pi(A'')$ Λ-doublet ratio is greater than 4 in the high-J limit, which also supports this impulsive model. All of these results support the well-established picture that the nonreacting OH or OD bond acts as a "spectator" in this reaction.

Introduction

The H + H_2O reactive system and its isotopically substituted analogs comprise one of the simplest systems in which there are several different vibrational modes of a polyatomic reactant. It may be the simplest such system that is tractable theoretically, because three of the four atoms are hydrogens, and experimentally, because of the stability and relative ease of handling the reactants or their precursors. As such, this system is of great importance in ongoing efforts to understand the dynamics of reactions of polyatomic molecules and the influence of vibrational excitation on these dynamics. This reaction may eventually serve as the prototype of a polyatomic reaction in much the same way as the H+ H_2 system serves as a prototype for triatomic reactions.[1]

The effect of reagent vibration on reactions of polyatomic molecules has received considerable attention.[2-4] Of particular interest are questions of bond selectivity and mode specificity: can the reaction rate or the yield of a desired product in a chemical reaction be increased by exciting a particular vibrational mode of a polyatomic reactant molecule? Early efforts to answer this question included both experimental and theoretical studies of several simple reactions, including Ba + $N_2O \rightarrow$ BaO + N_2,[5,6] O + $CS_2 \rightarrow$ CS + SO,[7-9] and NO + $O_3 \rightarrow NO_2 + O_2$.[10-12]

The reaction family

$$H + HOD \rightarrow OD(v,N) + H_2 \quad (1a)$$

$$OH(v,N) + HD \quad (1b)$$

and the related reactions

$$H + H_2O \rightarrow OH(v,N) + H_2 \quad (2)$$

$$H + D_2O \rightarrow OD(v,N) + HD \quad (3)$$

have proven particularly amenable to this type of study. Reactions 1–3 are endothermic, with a barrier estimated at 0.94 eV.[13] Thus, they require reactants with considerable excess energy, which can be present either as translational energy or internal excitation of the triatomic reagent.

Reaction 2 has been investigated extensively both experimentally[14-19] and theoretically.[20-25] Kleinermanns and Wolfrum[19] carried out the first quantum-state-specific dynamical study of this reaction, using H-atom translational energy to overcome the barrier. This and subsequent studies led to the conclusion that the reaction occurs by an H-atom abstraction mechanism; the nonreacting OH group acts as a "spectator", which is only weakly coupled to the other atoms in the collision complex and receives little of the energy available to the products. Schatz and Elgersma[24] constructed a potential energy surface for the H–H_2O system based on Walch and Dunning's[25] ab initio calculations for a set of geometries in the transition-state region. This surface has served as the basis for quasiclassical[22,23,26] and quantum mechanical[20,21,27-29] scattering calculations.

Reactions 1 and 2 have been used recently to investigate the effects of vibrational excitation on reactions. Crim and co-workers showed that reaction of thermal H atoms with HOD prepared with 4 quanta of OH vibrational excitation yields exclusively OD product (the observed OD:OH branching ratio was >100:1),[17,30] providing the first example of a bond-specific bimolecular reaction. They also studied the relative reaction rate as a function of H_2O vibrational state for reaction 2.[17] They found that preparing the

† Present address: Department of Chemistry, University of Wisconsin, Madison, 1101 University Avenue, Madison, WI 53706.

0022-3654/93/2097-2194$04.00/0

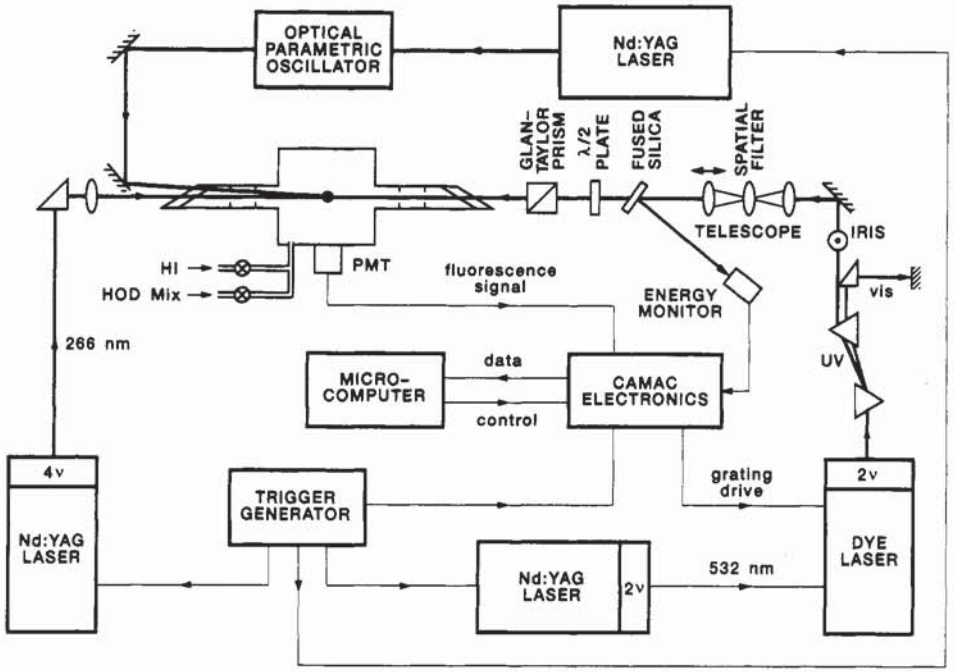

Figure 1. Schematic diagram of the experimental apparatus.

H_2O molecule in a (local mode) vibrational state with all its energy in the stretching of one bond enhanced the reaction rate much more than modes with some of the energy in other motions of the molecule, e.g., bend excitation or stretch excitation distributed between the two bonds. In both studies, most of the available energy was present as vibration of the triatomic, which was prepared in a high vibrational overtone state. It might be wondered whether the observed selectivity would persist at much lower levels of vibrational excitation, e.g., with only 1 quantum of vibration in the triatomic molecule and the remainder of the excess energy needed for reaction provided by reagent translation. A recent study in this laboratory of reaction 1[31] has answered this question in the affirmative and has provided the first example of the use of reagent vibrational excitation to select either of two possible sets of products in a chemical reaction.

In this paper we present a detailed study of the effect of polyatomic reagent vibrational excitation on reaction dynamics for reaction 1. The HOD molecule is prepared by infrared excitation with 1 quantum in either the OH or OD local mode stretch. For comparison, we also investigated the reaction of H atoms with ground-state HOD, H_2O, and D_2O. Our experiments with vibrationally excited reactant molecules are conducted at the lowest possible level of excitation (1 quantum). We show that large vibrationally mediated effects are observed nonetheless.

Experimental Section

Apparatus. A schematic of our experimental apparatus is shown in Figure 1. Our studies are carried out in a flowing mixture of HI, H_2O, HOD, and D_2O in the ratio 5:1:2:1 maintained at a total pressure of 50 mTorr. HOD is prepared in a selected vibrational state by infrared (IR) excitation using the output of a tunable optical parametric oscillator (OPO, 5–10-mJ pulse energy) pumped by the 1.064-μm fundamental from a Nd:YAG laser (Quanta-Ray DCR-1). H atoms are generated by photolysis of HI molecules with an ultraviolet (UV) laser pulse at 266 nm, the fourth harmonic of a Nd:YAG laser (Quantel 581-10, 10–15-mJ pulse energy). The pump and photolysis lasers are fired simultaneously, and their beams propagate collinearly into the reaction chamber. After a short, well-defined time delay (100 ns) a third tunable UV laser pulse, generated by frequency doubling the output of a Nd:YAG-pumped dye laser (Quantel TDL-50 pumped by a Quanta-Ray DCR-2A, 0.2 cm^{-1} UV bandwidth), counterpropagates through the chamber and probes the nascent OH and OD by laser-induced fluorescence (LIF) using the $A^2\Sigma^+$–$X^2\Pi$ ultraviolet band system in the spectral region 305–315 nm. The timing of the lasers is controlled by a digital pulse/delay generator (Stanford Research Systems DG535).

The OH and OD product signal that arises from reaction of H atoms with the vibrationally excited HOD is separated from that of other reactants (ground-state HOD, H_2O, and D_2O) using a shot-by-shot subtraction procedure. Both photolysis and probe lasers operate at a repetition rate of 20 Hz while the OPO fires at 10 Hz (i.e., on every other probe laser shot). By scanning slowly over OH and OD lines and subtracting LIF signals from alternate probe laser shots, we can separate background OH and OD signals not resulting from reaction of H atoms with vibrationally excited HOD. LIF excitation spectra are recorded in either of two probe laser scan modes: continuous scanning of probe wavelength or computer-controlled discrete scanning, which combines slow scans over OH and OD rotational lines with fast slewing between adjacent lines to minimize total scan time.

The fluorescence is collected perpendicular to the probe laser beam axis by a 2-in. fused silica plano-convex lens (at $f/1$), collimated through a UV bandpass interference filter (centered at 310 nm with 10 nm fwhm; Janos Technology), and focused by another 2-in. $f/1$ lens onto the photocathode of a photomultiplier tube (PMT; RCA C31034). Signals from the PMT are captured by a gated charge integrator (LeCroy 2249SG ADC, CAMAC modular data bus) during a time gate of 1.5 μs (corresponding to approximately twice the radiative lifetime of the OH and OD $A^2\Sigma^+$ state), delayed by 10–30 ns from the probe pulse to discriminate against scattered laser light. The digitized data are passed to a personal computer (IBM PC-XT) for storage and analysis.

The OPO and UV photolysis beams are brought to a loose focus of 3 mm in the LIF probe volume (the area viewed by the PMT). The 266-nm photolysis energy is attenuated to 10–15 mJ/pulse to minimize background fluorescence resulting from two-photon photolysis of HOD, H_2O, and D_2O to produce electronically excited (A state) OH and OD.[32] The probe beam is spatially filtered through a sapphire orifice and telescoped to overlap the photolysis and OPO beams (3-mm beam diameter). The probe laser energy is controlled with either two Glan-Taylor

polarizers or one polarizer and a half-wave plate centered at 308 nm and is monitored on a shot-to-shot basis by a power meter (Molectron J3-05) using a reflection off a fused silica plate.

The OPO was tuned to pump various vibrational transitions of HOD using an optoacoustic cell to locate features in the HOD IR excitation spectrum and a monochromator (1-m length with a 300 groove/mm grating; Spex, Model 1704) to verify the IR wavelength. The optoacoustic cell is fitted with a piezoelectric transducer (PCB Piezotronics Inc. Model GK106B50, together with a preamplifier Model 480D06) to detect acoustic waves and a capacitance manometer (MKS Baratron 122A, 0–10 Torr) to measure HOD pressure.

Our reaction chamber consists of a low-pressure stainless steel flow cell equipped with internally baffled entrance and exit arms (1.0 m long) and exhausted by a partially throttled oil diffusion pump. Reagent gases are introduced into the chamber through stainless steel needle valves, and the total pressure is monitored by a capacitance manometer (MKS Baratron 227, 0–1000 mTorr). HOD is generated by mixing (in a glass flask) equal volumes of liquid H_2O and D_2O (Aldrich, 99.9% D atom purity), which forms a statistical equilibrium mixture consisting of H_2O, HOD, and D_2O in the ratio 1:2:1. This mixture is degassed several times with a mechanical pump to remove dissolved gases (in particular O_2) before it is introduced into the reaction chamber. HI (Matheson, >98% purity) is further purified by freezing it in liquid nitrogen and pumping it, to remove any H_2 impurities. The HI reservoir was maintained at about −30 °C in a 3:2 water–ethanol slush bath to ensure a stable backing pressure and minimize contamination by gaseous I_2.

Experimental Conditions. The total pressure P and the pump–probe delay Δt (the time between firing of pump and probe lasers) are chosen to assure single-collision conditions: the product rotational distributions were observed to be invariant for $P\Delta t < 10^{-8}$ Torr s, and our data were collected with $P\Delta t = 5 \times 10^{-9}$ Torr s (50 mTorr total pressure, 100 ns pump–probe delay). Care was also taken to work at pressures low enough to avoid effects caused by quenching of the OH(OD) electronically excited A state during its fluorescence lifetime (approximately 700 ns[33]). For a given value of $P\Delta t$, the rotational distributions were found to be invariant for $P < 100$ mTorr.

The probe beam was set to overlap as closely as possible the photolysis and OPO beams, rather than having it significantly larger to illuminate all nascent products (as is usually done[34–36]). During our 100-ns time delay, fast (1.5 eV) H atoms will move 1.7 mm. Thus they can move significantly outside the area illuminated by the lasers, *where they can react only with HOD molecules that have not been optically excited.* That is, H atoms that fly out of the pump beams can produce only extra background OH and OD product. On the other hand, a nascent OH or OD molecule can move at most 0.3 mm, if it receives as translational energy all the product energy available. Hydroxyl products probably move considerably less than this; as spectators in the reaction, they are not expected to receive much of the available energy as translation. Thus, in overlapping the probe beam with the other two beams we lose negligible OD and OH product from H + excited HOD while we eliminate a significant source of background from H + unexcited HOD, H_2O, and D_2O.

Additional experiments were performed to determine at what probe laser energies the OH and OD A–X transitions were radiatively saturated. For unsaturated LIF, the height of a transition line profile is proportional to the product IB, where I is the laser intensity and B is the transition line strength (Einstein B coefficient), while the line width is independent of I and B.[37] For completely saturated LIF, the peak height is independent of I and B,[38] and the width is proportional to $(IB)^{1/2}$ because of power broadening.[39] Thus, the integrated line intensity is proportional to IB for unsaturated LIF and to $(IB)^{1/2}$ for saturated LIF.

To determine probe powers appropriate for unsaturated LIF, measurements were made of the ratios of intensities of main branch lines to those of the corresponding satellite branch lines (e.g., Q_1 and Q_{21}, Q_2 and Q_{12}). Such pairs of lines probe the same lower state but with substantially different transition line strengths. The intensity ratios were found to be independent of laser power at probe laser pulse energies less than 2.5 μJ (corresponding to a fluence of about 35 μJ/cm² over our 3-mm probe beam), indicating unsaturated detection of both main branch line and satellite at these energies. At higher probe pulse energies (>5 μJ/pulse), the intensity ratios increased with increasing laser power, indicating the onset of saturation (of the stronger main branch line).

To determine the power regime of completely saturated LIF, measurements of absolute integrated line intensity vs probe power were made on the strong P_1 branch of the OD(0,0) band. For probe energies in the range 50–200 μJ/pulse (700–2800 μJ/cm²), the line intensity varied as the pulse energy raised to the power 0.45 ± 0.05, in good agreement with the prediction for saturated LIF.

HOD Infrared Spectroscopy. HOD was pumped by tuning the OPO to strong features in the HOD absorption spectrum on either the (0,0,1) band (the OH stretch) at about 3800 cm^{-1} (2.65 μm)[40,41] or the (1,0,0) band (the OD stretch) at about 2800 cm^{-1} (3.57 μm).[40,42] Because the spacing of individual rotational lines in the HOD spectrum (0.1–0.7 cm^{-1}, average ~0.5 cm^{-1}) was less than the OPO bandwidth (1.0–1.5 cm^{-1}), single rotational levels of HOD could not be excited, and the unambiguous assignment of strong absorption features was difficult. To determine what rotational transitions were excited in the various features observed, HOD spectra were recorded and assigned in the following way.

The optoacoustic cell is filled with approximately 10 Torr of the H_2O–D_2O mix (giving 5 Torr of HOD) and pressurized to approximately 22 psi (1.5 atm) with argon, which increased the intensity of the acoustic waves. The OPO is then manually scanned over a spectral region of a strong HOD absorption, typically about 120 cm^{-1}, while the optoacoustic signal is recorded with our gated charge integrator. The OPO power is nearly constant over frequency regions of interest. The scanning is discrete: the OPO grating is moved manually approximately 0.4 cm^{-1} (about $^1/_3$ of the OPO bandwidth), then the integrator and computer record and sum the signal from 20 laser shots to give one point in the spectrum. Figure 2a shows a typical OPO spectrum acquired in this way, a section of the (1,0,0) ← (0,0,0) band of HOD.

These same spectral regions were simulated using the HOD absorption line positions and line strengths of Toth and Brault,[41,42] assuming a Gaussian OPO frequency profile. The Gaussian fwhm was adjusted to give the best fit to the observed spectrum; a typical bandwidth so calculated is 1.25 cm^{-1}. Figure 2b shows the simulated spectrum associated with the region scanned in Figure 2a. The agreement between the experimental and calculated spectra is good and permits assignment of the observed peaks.

Strong peaks for exciting HOD molecules were chosen to avoid overlap with D_2O lines,[43] which were identified and assigned as above using D_2O in the optoacoustic cell. Typical pumped features consisted of three unresolved rotational lines of one vibrational band, spanning one or two J values (in the range $J = 4$–5, the peak of the room temperature HOD Boltzmann distribution), with a variety of K_A and K_C quantum numbers. Thus, in our experiments, the vibrational level of HOD is exactly specified, the rotational level (J quantum number) is specified or defined within a narrow range, while the projection of J onto the molecular axes is not well defined. The rotational levels excited in each experiment are given in Table I.

HOD Vibrational Eigenstates. The OH and OD stretching

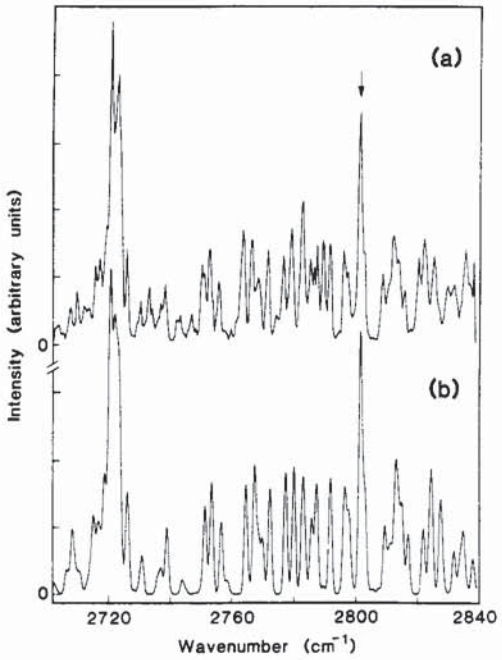

Figure 2. Sections of the (a) experimental and (b) simulated optoacoustic spectra of HOD in the region of the OD-stretch absorption. Spectrum b was simulated assuming an OPO bandwidth of 1.25 cm^{-1}. The match between strong absorption features of the two spectra is clear. In our experiments, HOD(1,0,0) was excited on the marked spectral feature.

TABLE I: HOD Rotational Excited Levels[a]

vibrational state	J'', K_A'', K_C''	J', K_A', K_C'	frequency (cm^{-1})
HOD(0,0,1)	4, 3, 2	5, 3, 3	3775.6651
	4, 3, 1	5, 3, 2	3776.3844
	4, 0, 4	5, 0, 5	3776.9001
HOD(1,0,0)	5, 1, 5	6, 1, 6	2801.4379
	4, 2, 2	5, 2, 3	2801.4729
	4, 1, 3	5, 1, 4	2801.6294

[a] The three levels in each case are not resolved.

vibrations of HOD are well-defined local modes even at the level of 1 quantum of excitation.[40,47] Reimers and Watts[47] calculated the expansion of the HOD vibrational eigenfunctions in a local mode basis set. They found that the OH vibrational eigenstate consists of 99% OH local mode basis function (i.e., the square of the coefficient for the OH local mode basis function in the expansion of this eigenstate is 0.99), which means that this state is almost a pure local mode. The OD vibrational eigenstate consisted of 86% of the OD local mode basis function. The authors do not state what basis function(s) gives the remaining 14%; most likely it is the doubly excited bend function, i.e., the H–O–D bend mode with 2 quanta of excitation, denoted (0,2,0). This state is nearly degenerate in energy with the OD local mode stretch state, at approximately 2700 cm^{-1}.

Bowman and co-workers have calculated the displacements of each of the three atoms in the normal mode vibrations of HOD.[48] They found that, for both HOD stretch modes, the extension of the bond between the O atom and the H or D atom in the "unexcited" bond was only about 7% of the extension of the "excited" bond. For a harmonic potential well, the energy in vibration of the unexcited bond is thus only $(0.07)^2 = 0.0049$ of that of the excited bond. Clearly, most of the energy in either stretch eigenstate is contained in vibration of only one bond.

Reaction Energetics. Figure 3 shows an energy level diagram for reaction 1. This reaction is endothermic by 0.66 eV (5320 cm^{-1})[44] and has an estimated barrier of 0.94 eV (7580 cm^{-1}).[13] The change in zero point energy between reactions 1a and 1b is small (~40 cm^{-1}).[45] One quantum of OH stretch provides approximately 0.47 eV (3800 cm^{-1}), and one quantum of OD

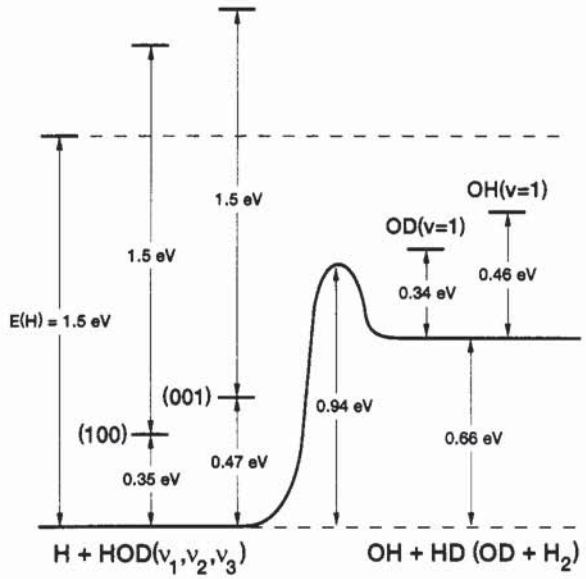

Figure 3. Energy level diagram for the reaction H + HOD → OH(OD) + HD(H_2).

stretch provides 0.35 eV (2800 cm^{-1}). The extra energy needed to overcome the barrier is provided by H-atom translational energy.

Photolysis of HI at 266 nm gives H atoms with two possible energies, 1.5 eV and 0.65 eV in the H–HOD center-of-mass frame (in the ratio 1.8:1[46]), because of the two possible spin–orbit states of the resulting I atom [I($^2P_{3/2}$) and I($^2P_{1/2}$)]. Only the 1.5-eV H-atom energy is indicated in Figure 3; however, the slower H atoms do have sufficient energy to overcome the barrier if the HOD molecule is vibrationally excited. The 1.5-eV H atoms have sufficient energy to react with both vibrationally excited and ground-state HOD, as well as H_2O and D_2O. This complication necessitates the use of the shot-by-shot subtraction procedure described above to separate signals that arise from reaction with vibrationally excited and ground-state reactants. It also allows us to study the reaction of H with ground-state HOD.

Results and Discussion

Because of the simplicity of the H + HOD system, the effects of vibrational excitation on this reaction are amenable to both intuitive understanding and detailed theoretical modeling. In this section we present measurements of product branching ratios, reaction cross sections, and hydroxyl product vibrational, rotational, and electronic fine-structure state distributions. The OD:OH branching ratios demonstrate that we can achieve laser-mediated bond-specific chemistry at the lowest possible level of vibrational excitation for the H + HOD reaction. Cross sections and vibrational branching ratios can be understood using simple classical models. The higher efficiency of stretch vibration over translational energy in promoting the reaction is as expected for a reaction with a late barrier. An impulsive model of energy release in the breakup of the H–HOD transition state accounts for most of the trends observed in hydroxyl product rotational and Λ-doublet fine-structure distributions. Finally, we compare our results to recent quasiclassical and quantum mechanical calculations of this system. We find that these theoretical efforts have achieved qualitative and in some cases quantitative agreement with experiment.

Data Acquisition and Analysis. OH and OD branching ratios and internal state distributions were obtained by recording laser-excitation spectra (fluorescence intensity vs probe laser wavelength) excited and detected on the (0,0) and (1,1) bands of the A–X electronic transition. Rotational lines in these spectra were assigned using the spectroscopic line position data of Dieke and

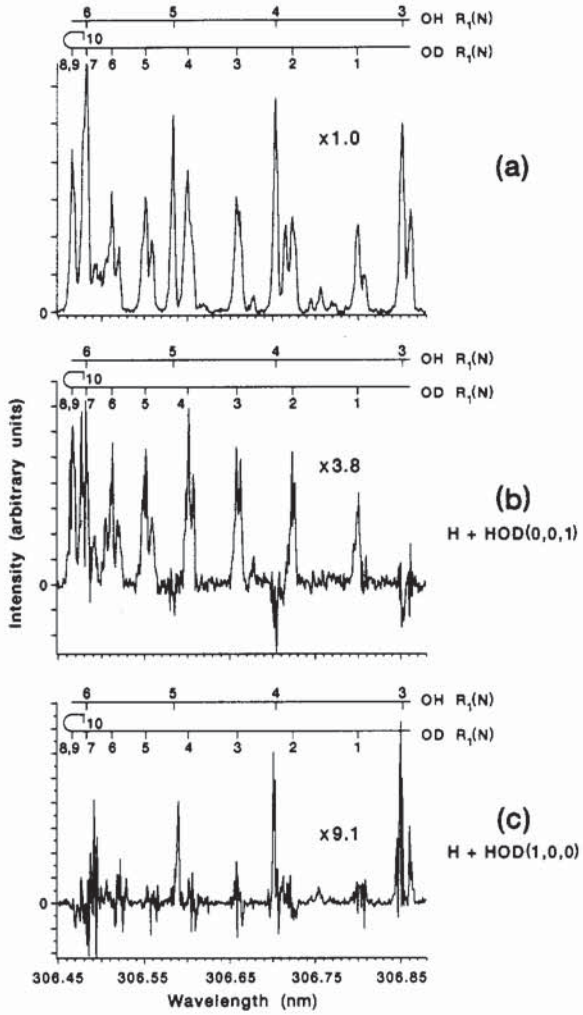

Figure 4. Segments of OH A–X and OD A–X LIF excitation spectra showing the hydroxyl products for the following reactions: (a) H + 1:2:1 mix of H_2O, HOD, D_2O; (b) H + HOD(0,0,1); and (c) H + HOD(1,0,0). The assignments of the R_1 branch lines of the OH(0,0) and OD(0,0) bands are indicated.

Crosswhite[49] for OH and those of Clyne, Coxon, and Woon Fat[50] for OD. Figure 4 shows representative spectra, which contain portions of the (0,0) band R_1 branches of the OH and OD products of the reaction of translationally hot H atoms with (a) the 1:2:1 ground-state mix of H_2O, HOD, and D_2O, (b) HOD excited with 1 quantum of O–H stretch, and (c) HOD excited with 1 quantum of O–D stretch. The spectra shown in Figure 4 parts b and c were obtained using shot-by-shot subtraction. Figure 4a shows that the reaction of fast H atoms with the ground-state mix produces substantial amounts of both OH and OD. In contrast, within our signal-to-noise level Figure 4b shows exclusively OD products from the reaction H + HOD(0,0,1) and Figure 4c shows exclusively OH products from the reaction H + HOD(1,0,0). Points of negative intensity, resulting from the subtraction procedure, disappear upon averaging over many scans.

Results for H + HOD(0,0,0), H + H_2O(0,0,0), and H + D_2O(0,0,0) were obtained by scanning the probe laser over the wavelength region common to both the OD and OH R_1 bands (see Figure 4a), without the use of the OPO or the subtraction procedure. Data on the reactions of H with H_2O and D_2O were obtained using the pure gases in the flowing reaction mixture. Data on H + HOD(0,0,0) were obtained by recording spectra with the 1:1 H_2O–D_2O mixture and subtracting from the recorded line intensities one-fourth of the intensities of corresponding lines of spectra acquired using pure H_2O or D_2O. This procedure is predicated on the statistical concentrations of reactants present in the 1:1 mixture, and it allows direct comparison of relative populations of OH and OD produced in the HOD reaction and determination of the OD:OH branching ratio.

Branching ratios and state distributions were obtained from analysis of many such spectra, recorded (except where noted) under unsaturated probing conditions and including (where appropriate) data for five of the six main spectroscopic branches: P_1, Q_1, R_1, P_2, and R_2. Integrated rotational line intensities were converted to relative populations by dividing by probe laser power, line strength (B coefficient), and a factor to account for the wavelength dependence of the interference filter transmission. Small corrections for the polarization of the probe laser, required when exciting LIF with linearly polarized light,[37] were also applied. The A and B coefficients used in this analysis were those calculated by Dimpfl and Kinsey.[33] Line intensities of spectra collected under saturated probing conditions were divided by the square root of the probe power and line strength, as discussed above.

OD:OH Branching Ratio. Analysis of multiple scans of spectra such as those shown in Figure 4 gave the following results for product branching ratios:

$$\text{OD:OH} = 1.38 \pm 0.14\text{:}1 \quad \text{for} \quad \text{H + HOD(0,0,0)} \tag{4a}$$

$$\text{OD:OH} > 25\text{:}1 \quad \text{for} \quad \text{H + HOD(0,0,1)} \tag{4b}$$

$$\text{OH:OD} > 5.8\text{:}1, <24\text{:}1 \quad \text{for} \quad \text{H + HOD(1,0,0)} \tag{4c}$$

These ratios take into account the $v = 0$ and $v = 1$ vibrational states of both major and minor hydroxyl products. In the case of HOD(1,0,0) a small amount of minor product was seen as OD(v=1) (see discussion of vibrational excitation below), which allows us to quote a maximum branching ratio; no OH(v=0) or OH(v=1) was observed for HOD(0,0,1). Our earlier report[31] of the branching ratios considered only $v = 0$ product. The limits on the branching ratios for excited HOD are determined from the signal seen for the major hydroxyl product and the signal (if any) and 1-σ error in the signal of the minor product; this 1-σ uncertainty was always substantial because of subtraction noise.

On a fundamental level, the preference to form one product or the other depending on the excitation of the HOD molecule is remarkable. In our experiments, most of the reactants' energy comes from H-atom translational energy. HOD vibrational excitation accounts for less than 25% of the total energy available. By contrast, most of the energy in the experiments of Crim and co-workers[15,17,18,30] was provided by H_2O or HOD vibrational excitation. Equation 4a shows that when *all* the energy comes from H-atom translation, the result is approximately "statistical": the O–H and O–D bonds are broken nearly equally often. Equations 4b and 4c demonstrate that even a relatively small increase in the total available energy can have a dramatic and highly nonstatistical effect on the products, depending on how that energy is deposited in the reactants. These experiments demonstrate above all else that the way energy is put into a reaction can make a great difference in how that reaction proceeds.

Relative Cross Sections for the Reaction of Excited and Unexcited HOD. The higher limit on the branching ratio in reaction 4b compared with that of reaction 4c reflects the higher signal-to-noise ratio for the major product in this experiment. This difference can also be seen by comparing the spectra in Figure 4 parts b and c, and it results from the much larger OPO-induced signal for OH-stretch pumping than for OD-stretch pumping. Since the OPO pumping efficiencies are comparable for the two experiments, this observation suggests that the enhancement in reaction cross section is considerably larger for OH-stretch excitation than for OD-stretch excitation, a conclusion borne out by the following more detailed considerations.

Comparison of the relative LIF signal intensities that result from excited vs unexcited HOD molecules allows us to estimate the relative reactive cross sections for vibrationally excited HOD.

TABLE II: Relative Reaction Cross Sections

precursor	prod	rel cross section	precursor	prod	rel cross section
$H_2O(0,0,0)$	OH	1.00 ± 0.02	HOD(0,0,0)	OD	0.47 ± 0.03
$D_2O(0,0,0)$	OD	0.37 ± 0.02	HOD(0,0,1)	OD	>9.40
HOD(0,0,0)	OH	0.34 ± 0.04	HOD(1,0,0)	OH	>1.70

This calculation takes into account the fraction of the HOD molecules in the rotational states being pumped (typically 6–7%) and an estimate of the pumping efficiency, or fraction of these molecules that are actually excited. The fraction excited depends on the line strengths of the transitions and the bandwidth and photon fluxes (energies) available from the OPO. Our calculations suggest that we are partially saturating the HOD excitation transitions; typical calculated excitation efficiencies are 30–40%, i.e., nearly the maximum possible efficiency of 50%. The actual number of HOD molecules excited in our experiments is probably consideraly less than the calculation suggests; factors such as shot-to-shot spatial jitter and losses on beam steering and focusing optics can greatly reduce the pumping efficiency for molecules in the LIF probe volume. Thus, the cross section enhancements we quote here are lower limits on the true enhancements.

Denoting by σ_{OH} and σ_{OD} the cross sections for formation of OH and OD from HOD, respectively, we find that

$$\sigma_{OD}(HOD(0,0,1))/\sigma_{OD}(HOD(0,0,0)) > 20 \quad (5a)$$

$$\sigma_{OH}(HOD(1,0,0))/\sigma_{OH}(HOD(0,0,0)) > 5 \quad (5b)$$

We can also estimate relative reaction cross sections for the three ground-state species $H_2O(0,0,0)$, $D_2O(0,0,0)$, and HOD-(0,0,0) by comparing LIF intensities observed in scans using H_2O, D_2O, and the 1:1 mix under conditions of constant total pressure and laser powers. Table II summarizes our measurements of the relative reactive cross sections of excited and unexcited HOD, as well as H_2O and D_2O. All cross sections have been normalized to that of $H + H_2O(0,0,0)$. Kessler and Kleinermanns[14] recently measured the absolute reactive cross section for this reaction at a variety of H-atom translational energies, including energies close to those used in this study. They measured $\sigma_{OH}(H_2O(0,0,0))$ to be 0.17 ± 0.07 Å^2 at an H-atom collision energy of 1.4 eV.

The excited-state reactive cross sections and OD:OH branching ratios quoted above indicate that vibrational excitation of either the OH or OD stretch greatly increases the probability of a fast H atom to break the excited bond. A simple model that gives qualitative understanding and insight into this observation, and into the dependence of reactivity on the H-atom approach angle, is given in Figure 5. Figure 5a shows the reaction of an H atom with ground-state HOD. This model assumes that to abstract an H (or D) atom, a fast H atom must strike the bound atom with sufficient energy directed along the bond (the reaction coordinate) to cause reaction, i.e., the H atom must approach at a sufficiently small angle for reaction to occur. This requirement leads to a restricted set of approach velocities, bounded by the *cone of acceptance* (also indicated in Figure 5), that can lead to reaction. Since the bond strengths of OH and OD are nearly equal, the cones of acceptance for these bonds and the probabilities for the two bonds to react will be similar. Vibrational excitation of either bond increases the energy along the reaction coordinate for cleavage of that bond. In this case, impinging H atoms do not need to have as much of their energy along the bond axis for reaction to occur, which means they can strike at higher angles. The cone of acceptance is thus widened by vibrational excitation (Figure 5b), so that a larger number of possible H-atom trajectories will result in reaction. The reaction probability and cross section of the excited bond are increased accordingly. This model will be especially useful in interpreting hydroxyl product rotational distributions.

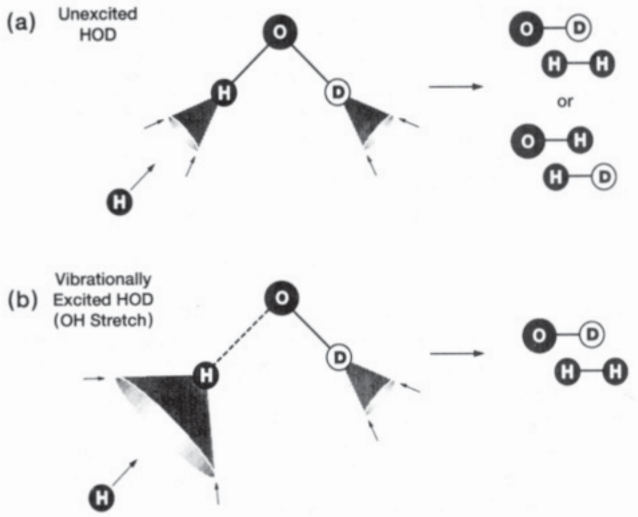

Figure 5. The cone-of-acceptance model for the reaction H + HOD. For unexcited HOD (a), only a narrow range of H-atom velocity vectors, those that lie inside the cone, can lead to reaction. Vibrational excitation widens the cone of acceptance (b), so that many more H-atom velocity vectors will lead to reaction, and the probability of reaction increases.

Efficiency of Vibration vs Translation in Promoting Reaction. Our results and those of Kessler and Kleinermanns show that vibrational energy increases the cross section of the H + HOD reaction considerably more than would an equivalent amount of energy in translation. Equation 5 shows that increasing the vibrational energy of HOD by 0.47 or 0.35 eV increases the cross section by at least a factor of 20 or 5, respectively. On the other hand, Kessler and Kleinermanns[14] found that the cross section of $H + H_2O$ is approximately constant with H-atom energy for energies above the barrier: the cross section increases only about 40% when the H-atom kinetic energy is increased from 1.4 to 2.6 eV, which implies increases of approximately 16% or 12% from an extra translational energy of 0.47 or 0.35 eV. Clearly, excitation of stretching vibration enhances the reactivity considerably more than additional translational energy: 1 quantum of OD or OH stretch is more effective at promoting reaction than the equivalent extra kinetic energy by factors of at least 30 and 120, respectively. Equation 4a suggests that even the difference in zero point energy between the OH and OD bonds (about 500 cm^{-1} = 0.06 eV) increases the reactivity of OH over OD by approximately 40%.

These observations are consistent with the picture developed by Polanyi and co-workers[2,51,52] for the effects of vibrational vs translational energy on reactivity in atom–diatom reactions: vibrational energy is more effective at overcoming late barriers, whereas translation is more effective at overcoming early barriers. These effects have been observed for a number of triatomic systems,[53-56] and it might also be expected that these ideas apply to the endoergic four-atom $H–H_2O$ reaction system because the nonreacting H atom is not strongly coupled to the reaction. In the calculated $H + H_2O$ transition state,[24] the forming H_2 bond is 13% longer than the equilibrium H_2 bond length, whereas the breaking OH bond is 36% longer than its equilibrium length. At the saddle point, then, the molecules resemble the products much more than the reactants, and so the reaction has a late barrier, as would be anticipated for an endoergic reaction. We thus expect that vibration is more effective than translation at overcoming this barrier to reaction, which is what is observed.

Product Vibrational Excitation. For each HOD vibrational mode studied, we checked for the formation of OH(v=1) and OD(v=1) by scanning the probe laser over the R_1 branches of the (1,1) vibrational bands of these species. Spectra of the v = 1 regions were recorded using saturated probe power conditions because of the considerably higher signal-to-noise level available in this mode. Table III lists the observed percent yield of

TABLE III: Percent Yields of Vibrationally Excited OH and OD

species	precursor	percent yield	(v=0):(v=1)ratio
OD(v=1)	HOD(1,0,0)	5.0 (+2.8, –0.8)	20 (+4, –7)
	HOD(0,0,0)	<0.62	>160:1
	D_2O(0,0,0)	<2.7	>35:1
	HOD(0,0,1)	<2.3	>45:1
OH(v=1)	HOD(0,0,0)	<0.33	>300:1
	H_2O(0,0,0)	<0.54	>185:1
	HOD(0,0,1)	<1.6	>65:1

vibrationally excited products. In only one case, H + HOD(1,0,0), was any vibrational excitation observed. In all other experiments the quoted limit reflects the ratio of observed $v = 0$ product signal to the estimated uncertainty in the zero of the $v = 1$ signal. The lack of any observable vibrationally excited product in the reactions of ground-state HOD, H_2O, and D_2O further reinforces the picture of the nonreacting bond as a spectator and shows specifically that the coupling between the hydroxyl vibrational motion and the rest of the collision complex is very small.

Crim and co-workers have shown that vibrational excitation of the spectator group is preserved as hydroxyl product vibrational excitation. They observed that the reaction

$$H + H_2O|1,3\rangle^- \rightarrow H_2 + OH$$

yields primarily (89%) OH(v=1) when the H_2O is prepared in a (local mode) vibrational state with 3 quanta in one stretch vibration and 1 quantum in the other.[17] On the other hand, when H_2O is prepared in the nearly isoenergetic $|0,4\rangle^-$ state, with 4 quanta in one stretch and zero in the other, nearly all the OH product is formed with $v = 0$ [3% OH(v=1)],[15] which indicates that the product vibrational excitation in the former case arises from spectator OH vibration in the H_2O reactant rather than from excitation during the reaction. These observations suggest that cleavage of the nonexcited bond in the reaction of HOD-(1,0,0) or HOD(0,0,1) would leave the hydroxyl product primarily in the state $v = 1$. This inference implies that the ratio of the reaction cross sections of the excited and unexcited bonds of HOD is equal to the ratio of ground-state product resulting from the unexcited bond to the vibrationally excited ($v = 1$) product from the excited bond. Specifically, from Table III we predict that in the reaction H + HOD(1,0,0) the cross section for cleavage of the excited OD bond is approximately 20 times larger than that of the OH bond, and thus the OH:OD bond selectivity is about 20:1, whereas in the reaction H + HOD(0,0,1), the cross section enhancement of the OH bond over OD and the OD:OH ratio are greater than 65. If the spectator vibrational state is preserved under our experimental conditions, the true branching ratios may be close to these estimates because the nonlocal character of the OD and OH stretch modes of HOD is small or insignificant.

OH and OD Rotational Distributions. Figures 6 and 7 show the observed rotational state distributions for the OH(v=0) and OD(v=0) products of the reaction of fast H atoms with HOD-(0,0,0), HOD(0,0,1), HOD(1,0,0), D_2O(0,0,0), and H_2O(0,0,0). The OD(v=1) from HOD(1,0,0) appeared to have approximately the same rotational distribution as OD(v=0) from HOD(0,0,1), but signal levels for OD(v=1) were too low to obtain a detailed population distribution. Our distribution for OH(v=0) from H_2O is in agreement with those observed by Honda et al.[16] at an H-atom translational energy of 1.5 eV and Kessler and Kleinermanns[14] at 1.4 eV. Rotational distributions from vibrationally excited HOD were derived from intensities of P_1 branch members, most of which were free from overlap. The ground-state distributions were derived from intensity data recorded on the R_1 branch: the OH and OD R_1 branches lie within a relatively small probe laser wavelength range (306.3–307.2 nm; see Figure 4), so that scanning over this region provided both rotational distributions and the OD:OH branching ratio. Congestion in the R_1 bandhead region,

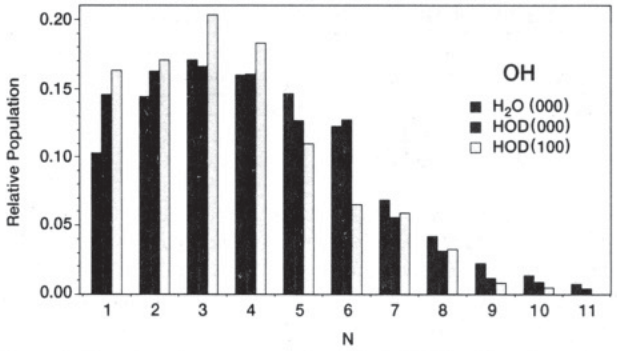

Figure 6. Rotational state populations of the OH(v=0) products from the reaction of 1.5 eV H atoms with HOD(1,0,0), HOD(0,0,0), and H_2O. Shown are N-state distributions of the A′ Λ-doublet of the $^2\Pi_{3/2}$ spin–orbit component. All distributions have been normalized to have a total population of unity.

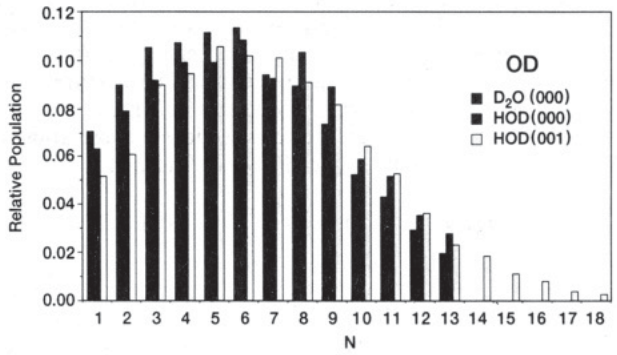

Figure 7. Rotational state populations of the OD(v=0) products from the reaction of 1.5-eV H atoms with HOD(0,0,1), HOD(0,0,0), and D_2O, as in Figure 6.

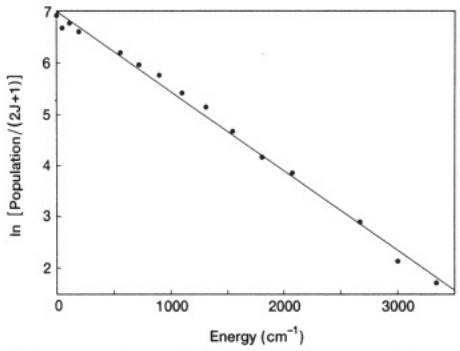

Figure 8. Boltzmann plot of the rotational state population distribution of the OD(v=0) product from the reaction of 1.5-eV H atoms with HOD-(0,0,1).

however, led to overlap between some pairs of R_1 rotational lines. Individual state populations were deduced from the sum intensities of blended lines, as discussed below.

All rotational distributions could be fit satisfactorily to a Boltzmann distribution, i.e., a distribution of the form $P(J) = (2J + 1)\exp(-E_J/kT)$, for some T. For example, Figure 8 shows a Boltzmann plot of the distribution of the OD product from HOD(0,0,1), which is well described by a straight line, implying a temperature. Populations of the OD rotational levels $N = 5$, 6, and 15 were deduced from this plot: these P_1 lines of OD were overlapped with other lines so that their intensities could not be measured. For R_1 branch intensity distributions containing overlapped lines, rotational populations and temperatures were deduced by comparing the observed intensities to distributions calculated assuming a Boltzmann distribution and then varying the temperature until the best fit was obtained. Individual state populations were then determined from the observed blended line intensities using the ratios of the contributions of individual lines to these intensities as given by the best-fit Boltzmann

TABLE IV: Rotational Temperatures of OH and OD Products

species	precursor	rotational temp[a]	species	precursor	rotational temp[a]
OD(v=0)	HOD(0,0,1)	922 ± 40	OH(v=0)	HOD(1,0,0)	555 ± 23
	HOD(0,0,0)	1030 ± 75		HOD(0,0,0)	675 ± 75
	D_2O(0,0,0)	850 ± 75		H_2O(0,0,0)	750 ± 75

[a] Derived for the A′ Λ-doublet component of the $^2\Pi_{3/2}$ spin–orbit state.

distribution. Table IV gives the best fit rotational temperatures for all observed distributions. Honda et al. measured T_{OH} = 800 ± 50 K for H + H_2O, in agreement with our measurement of T_{OH} = 750 ± 75 K.

The rotational distributions of Figures 6 and 7 are "cold"; average rotational energies are 400–700 cm^{-1}, or 0.05–0.085 eV, compared with available reaction product energies of 0.84 eV–1.31 eV. This observation is consistent with the results of many previous investigations[14-19] and further supports the picture of the nonreacting OH or OD fragment as a spectator.

The rotational distributions and temperatures given above exhibit several trends. The most striking is that OD fragments invariably receive more rotational energy than OH fragments: the average rotational temperature of the OD products is 930 vs 660 K for OH. This difference can be understood using a simple impulsive model for the breakup of the collision complex. The breaking of the OH or OD bond will rotationally excite the remaining hydroxyl fragment by exerting a force on the O atom and hence a torque on the molecule. The magnitude of this torque depends on the lever arm on which the force acts, i.e., on the distance of the O atom from the center of mass of the hydroxyl molecule (which is larger for OD than OH). Specifically, the rotational energy imparted will be proportional to the reduced mass of the molecule, $\mu_{OH} = m_O m_H/(m_O + m_H)$. The ratio μ_{OD}/μ_{OH} is 1.89 ($\sim m_D/m_H$), which is somewhat larger than the ratio of the observed rotational temperatures of OD and OH. However, the difference in the position of the center of mass in OD vs OH does qualitatively account for this result.

Other mechanisms of product hydroxyl rotation, such as thermal rotational motion of the triatomic and bending motion of the HOD molecule (zero point or otherwise), predict approximately equal rotatioinal energy of OH and OD products. Repulsion between the hydroxyl hydrogen and the forming H_2 or HD molecule should give higher rotational excitation of OH products than OD products because the H atom is lighter. Only repulsion between the atoms of the breaking OH or OD bond correctly predicts the observed higher rotational excitation of OD fragments, suggesting that such repulsion is the main source of rotational excitation of the product hydroxyl fragment.

The rotational temperature of both OH and OD also varies, depending on the precursor molecule and its preparation. We hesitate to attach too much significance to these differences because they are not much larger than the experimental uncertainties in these measurements. However, there does appear to be a trend in the rotational temperatures of the products from HOD: vibrational excitation of either bond leads to a hydroxyl product with less rotational energy than the ground-state molecule gives. This somewhat surprising result can be understood using the cone-of-acceptance model described above. Departing molecular hydrogen products from wide-angle H- or D-abstracting collisions would be expected on average to exert less force perpendicular to the nonreacting bond axis, and hence apply less torque on the OH or OD, than would "head-on" narrow-angle collisions. Hydroxyl products from vibrationally excited HOD would thus receive less rotational excitation, on average, than would the same products from ground-state HOD.

Either hydroxyl product also appears to receive less rotational energy when a D atom is abstracted than when an H atom is abstracted. Specifically, H + D_2O leaves the OD with less energy than H + HOD, and H + HOD leaves OH with less energy than H + H_2O. This result is somewhat puzzling; an impulsive model suggests that a departing D atom would exert a larger impulse on the hydroxyl group than a departing H atom because of the larger mass of D. The relative impulse from H vs D atoms appears to be governed by more subtle dynamical factors than such simple models can account for.

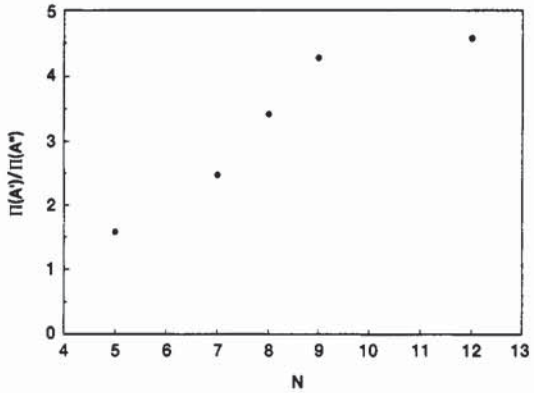

Figure 9. Λ-doublet population ratios, A′/A″, as a function of N, for the OD(v=0) product of the reaction H + HOD(0,0,1) at 1.5 eV.

Electronic Fine-Structure Distributions. By measuring the intensities of pairs of $P_1(N)$ and $Q_1(N)$ lines, we have determined the Π(A′)/Π(A″) Λ-doublet ratio for several rotational states of the OD product of the reaction H + HOD(0,0,1) → OD + H_2. Because of overlap of OD Q_1 lines with OH lines it was not possible to study systematically the Λ-doublet ratio for the reaction with ground-state HOD. In OH and OD the Λ-doublet components are defined by the orientation of the singly occupied pπ orbital on the O atom with respect to the plane of rotation of the molecule: for the A′ component, this orbital lies in the plane of rotation, while in the A″ component the pπ orbital is perpendicular to this plane. Our results are shown graphically in Figure 9. We see that the A′/A″ ratio increases monotonically with rotational quantum number to a maximum of greater than 4 for high N. At low N the ratio appears to decrease to near unity, as expected; for low N values the Λ-doublet components do not describe the pπ orbital lying parallel or perpendicular to the plane of rotation; rather they are linear combinations of these two limiting orientations. Honda et al.[16] and Kleinermanns and Wolfrum[19] observed similar trends in the Λ-doublet distributions of the OH product from H + H_2O, with ratios of 2.6 ± 0.2 and 3.2 ± 1.0, respectively, at high N. Because the Λ-doublet ratio changes with N, the rotational temperatures of the two Λ-doublet components should be different, an effect noted by Honda et al.[16]

The O-atom pπ orbital correlates asymptotically with the broken O–H bond, and its orientation with respect to the plane of rotation should correlate with the rotation of the OD fragment during the breaking of that bond. Two factors that could influence the angular motion of the OD with respect to the breaking bond are forces on the O atom and forces on the D atom. More specifically, the breaking of the O–H bond will cause a force to be exerted on the O atom, which will give rise to a torque on the OD molecule, as discussed earlier. The force will be along the direction of the bond, so that the torque and resulting angular momentum will be perpendicular to this bond. Asymptotically, then, the plane of rotation of the molecule will contain the broken bond (or singly occupied orbital), which corresponds to the A′ Λ-doublet.

The Λ-doublet propensities could also be influenced by angular motion of the D atom with respect to the O atom (i.e., OD rotation) during breakup of the collision complex. Such motion could be caused by either random (thermal) motion of the OD bond before or during the collision, which would give rise to a 2:1 Λ-doublet ratio,[57] or forces on the D atom by the departing H_2 molecule during breakup. These latter forces would most likely cause rotation in the H–O–D plane (the H–H–O–D transition state is

planar[24,25]) and hence in a plane containing the breaking OH bond, which would likewise favor the A′ Λ-doublet. As discussed earlier, these factors are unlikely to make as large a contribution to OD rotation as H–O repulsion, so such repulsion is likely the main source of the large preference for formation of the in-plane A′ Λ-doublet component.

Leone and co-workers[58] recently observed preferential alignment of H_2O molecules in the inelastic scattering of fast H atoms by H_2O. They found that scattering events produced rotationally excited $H_2O(0,0,1)$ predominantly with $J = K_C$, i.e., with J oriented perpendicular to the plane of the H_2O molecule. They suggested this preference for in-plane rotation might arise because only H atoms that approached in the plane of the H_2O molecule would excite the asymmetric stretch vibration, whereas out-of-plane collisions would tend to excite rotations. Alternately, the in-plane rotation could be caused by "failed-reactive" collisions that formed the H–H–O–H transition state but did not continue to form OH + H_2 products. The breakup of this transition state to form H + H_2O would occur with impulsive energy release as discussed above for the reactive collision, and since the H–H–O–H transition state is planar, this breakup would result in in-plane H_2O rotation. This mechanism is analogous to the one we propose above to account for in-plane rotation of the products of reactive collisions.

We also measured the $^2\Pi_{3/2}$:$^2\Pi_{1/2}$ spin–orbit ratio for several rotational states of the OH(v=0) and OD(v=0) products of the reaction of hot H atoms with HOD(0,0,1), HOD(0,0,0), H_2O, and D_2O by measuring the intensities of pairs of $P_1(N)$ and $P_2(N)$ or $R_1(N)$ and $R_2(N)$ lines. We observed a significant preference in all cases for population of the lower energy $^2\Pi_{3/2}$ state. Typically, a rotational level of the $^2\Pi_{1/2}$ electronic state had 65–90% of the population of the same rotational level of the $^2\Pi_{3/2}$ state, with both state populations divided by their respective $2J + 1$ degeneracies. No strong dependence of the spin–orbit ratio on rotational level, species (OH or OD), precursor, or precursor vibrational state was observed. In a completely statistical distribution, the populations of the two spin–orbit states would differ only slightly: typical spin–orbit splittings are 150–350 cm^{-1},[59] compared with 6700–10 500 cm^{-1} of energy available to the products. These observations suggest a slight preference for reaction on an electronic fine structure potential energy surface that correlates with the $^2\Pi_{3/2}$ electronic state of the OH(OD) product.

Comparison to Theory

Following the early work of Schatz and co-workers,[22] recent theoretical studies of the dynamics of the H + HOD reaction have involved calculation of the absolute reaction cross section for the production of various product species and quantum states.[26-29] Investigated quantities include cross section enhancements,[26,28] OD:OH branching ratios,[26-28] product vibrational excitation,[27,29] and OD product rotational distributions,[29] all as a function of the initial vibrational state of the HOD molecule. The potential energy surface available for this system is an analytic fit by Schatz and Elgersma[24] to the ab initio points calculated by Walch and Dunning.[25] On this surface only one of the H atoms of H_2O is "reactive" and can be abstracted, so that for HOD calculations the abstracted atom was determined in advance.

Using this surface, Kudla and Schatz[26] carried out quasiclassical trajectory studies of the H + HOD reaction at many H-atom energies, including 1.5 eV. Wang and Bowman[28] performed reduced dimensionality quantum scattering calculations of rotationally averaged cross sections for this reaction at a variety of H-atom translational energies including 1.5 eV. Table V summarizes the OD:OH branching ratios and cross section enhancements calculated in these studies. In addition, Clary[29] performed quantum scattering calculations on only one of the two reaction channels, H + HOD → OD + H_2, at H-atom collision energies up to approximately 1 eV. He found that, at these energies, σ_{OD} is larger by a factor of 5 for HOD(0,0,1) than for HOD(1,0,0), and the yield of OD(v=1) from HOD(1,0,0) is much greater than that from HOD(0,0,1). He also determined the OD(v=0) rotational distribution for H + HOD(0,0,1); it is qualitatively similar to the distribution we measured but somewhat colder, with a peak at $J = 0$.

TABLE V: Comparison of Theoretical and Experimental Results for the Reaction H + HOD at 1.5 eV H-Atom Energy

reactant	method[a]	OD:OH	cross section enhancement[b]	ref
HOD(0,0,1)	QM	14:1	19	28
HOD(1,0,0)	QM	1:2.8	21	28
HOD(0,0,0)	QM	1.5:1		28
HOD(0,0,1)	QCT	8.5:1	7.1	26
HOD(1,0,0)	QCT	1:3.1	9.1	26
HOD(0,0,0)	QCT	2.5:1		26
HOD(0,0,1)	expt	>25:1	>20	this work
HOD(1,0,0)	expt	<1:5.8, >1:24	>5	this work
HOD(0,0,0)	expt	1.38 ● 0.14:1		this work

[a] QM, quantaum mechanical scattering; QCT, quasiclassical trajectory calculations. [b] Enhancement in cleavage of the excited bond (calculated from the data given).

The theoretical results are in qualitative agreement with our experimental results. All calculations showed large enhancements in the reactivity of a vibrationally excited OH or OD bond and considerable specificity in the formation of products depending on which bond was excited. In some cases [e.g., quantum calculations on HOD(0,0,0)] theory and experiment approach quantitative agreement, but not in general. Theory often underestimates the magnitude of the bond specificity. The calculated cross section enhancements and rotational distributions are likewise in qualitative but not quantitative agreement with experiment. This lack of agreement may stem from two sources: the imprecise nature of the potential energy surface used in the calculations, e.g., unphysical wells and bumps known to exist in the asymptotic region,[24,60] and the approximations used in carrying out the scattering dynamics on this surface. We hope that the present experimental results will stimulate further theoretical efforts to model this system.

Conclusion

We have presented a detailed study of the effects of vibrational excitation on the title reaction. We find a high degree of bond specificity: vibrational excitation of a particular bond leads to a large enhancement in the reactive cleavage of that bond and hence to a large shift in the product branching ratio toward production of the products of that bond cleavage. This shift in branching ratio, as well as measured reactive cross section enhancements and vibrational branching ratios, can be qualitatively understood using a cone-of-acceptance model. The higher efficiency of vibrational stretch excitation over extra translational energy in promoting reaction is as expected for the H + HOD reaction because this endothermic reaction has a late barrier. Impulsive models correctly predict most of the observed trends in the hydroxyl product rotational distributions and Λ-doublet ratios. Comparing these results with recent theoretical calculations, we find qualitative but not quantitative agreement. Refinement of the available potential energy surface or further development of the techniques of the dynamical calculations should facilitate the accurate simulation of this example of bond-specific chemistry, which may be the simplest reaction involving an atom and a triatomic molecule.

Acknowledgment. We thank B. Girard and R. Zhang for valuable technical assistance in the early stages of this work. M.J.B. gratefully acknowledges a GAANN graduate fellowship

from the U.S. Department of Education. W.R.S. thanks the National Science Foundation for a graduate fellowship. This work was supported by the National Science Foundation Grant No. NSF CHE 89-21198.

References and Notes

(1) Marinero, E. E.; Rettner, C. T.; Zare, R. N. *J. Chem. Phys.* **1984**, *80*, 4142. Gerrity, D. P.; Valentini, J. J. *J. Chem. Phys.* **1983**, *79*, 5202.
(2) Levine, R. D.; Bernstein, R. B. *Molecular Reaction Dynamics and Chemical Reactivity*; Oxford University Press: New York, 1987.
(3) Wolfrum, J. In *Reactions of Small Transient Species: Kinetics and Energetics*; Fontijn, A., Clyne, M. A. A., Eds.; Academic Press: London, 1983; Chapter 3.
(4) Crim, F. F. *Annu. Rev. Phys. Chem.* **1984**, *35*, 657.
(5) Jalink, H.; Harren, F.; van den Ende, D.; Stolte, S. *Chem. Phys.* **1986**, *108*, 391.
(6) Wren, D. J.; Menzinger, M. *Faraday Discuss. Chem. Soc.* **1979**, *67*, 97.
(7) Schatz, G. C. *J. Chem. Phys.* **1979**, *71*, 542.
(8) Elgersma, H.; Schatz, G. C. *Chem. Phys.* **1981**, *54*, 201.
(9) Schatz, G. C.; Moser, M. D. *Chem. Phys.* **1978**, *35*, 239.
(10) Bar-Ziv, E.; Moy, J.; Gordon, R. J. *J. Chem. Phys.* **1978**, *68*, 1013.
(11) Chapman, S. *J. Chem. Phys.* **1981**, *74*, 1001.
(12) Hui, K. K.; Cool, T. A. *J. Chem. Phys.* **1978**, *68*, 1022.
(13) Truhlar, D. G.; Isaacson, A. D. *J. Chem. Phys.* **1982**, *77*, 3516. Isaacson, A. D.; Truhlar, D. G. *J. Chem. Phys.* **1982**, *76*, 1380.
(14) Kessler, K.; Kleinermanns, K. *Chem. Phys. Lett.* **1992**, *190*, 145.
(15) Hsiao, M. C.; Sinha, A.; Crim, F. F. *J. Phys. Chem.* **1991**, *21*, 8263.
(16) Honda, K.; Takayanagi, M.; Nishiya, T.; Ohoyama, H.; Hanazaki, I. *Chem. Phys. Lett.* **1991**, *180*, 321.
(17) Sinha, A.; Hsiao, M. C.; Crim, F. F. *J. Chem. Phys.* **1991**, *94*, 4928.
(18) Sinha, A. *J. Phys. Chem.* **1990**, *94*, 4391.
(19) Kleinermanns, K.; Wolfrum, J. *Appl. Phys. B* **1984**, *34*, 5.
(20) Wang, D.-S.; Bowman, J. M. *J. Chem. Phys.*, in press.
(21) Clary, D. C. *J. Chem. Phys.* **1991**, *95*, 7298.
(22) Schatz, G. C.; Colton, M. C.; Grant, J. L. *J. Phys. Chem.* **1984**, *88*, 2971.
(23) Elgersma, H.; Schatz, G. C. *Int. J. Quantum Chem., Symp.* **1981**, *15*, 611.
(24) Schatz, G. C.; Elgersma, H. *Chem. Phys. Lett.* **1980**, *73*, 21.
(25) Walch, S. P.; Dunning, T. H., Jr. *J. Chem. Phys.* **1980**, *72*, 1303.
(26) Kudla, K.; Schatz, G. C. *Chem. Phys. Lett.* **1992**, *193*, 507.
(27) Bowman, J. M.; Wang, D.-S. *J. Chem. Phys.* **1992**, *96*, 7852.
(28) Wang, D.-S.; Bowman, J. M. Unpublished work.
(29) Clary, D. C. *Chem. Phys. Lett.* **1992**, *192*, 34.
(30) Sinha, A.; Hsiao, M. C.; Crim, F. F. *J. Chem. Phys.* **1990**, *92*, 6333.
(31) Bronikowski, M. J.; Simpson, W. R.; Girard, B.; Zare, R. N. *J. Chem. Phys.* **1991**, *95*, 8647.
(32) Atkins, C. G.; Briggs, R. G.; Halpern, J. B.; Hancock, G. *Chem. Phys. Lett.* **1988**, *152*, 81.
(33) Dimpfl, W. L.; Kinsey, J. L. *J. Quant. Spectrosc. Radiat. Transfer* **1979**, *21*, 233.
(34) Zhang, R.; van der Zande, W. J.; Bronikowski, M. J.; Zare, R. N. *J. Chem. Phys.* **1991**, *94*, 2704.
(35) Bronikowski, M. J.; Zhang, R.; Rakestraw, D. J.; Zare, R. N. *Chem. Phys. Lett.* **1989**, *156*, 7.
(36) McKendrick, K. G.; Rakestraw, D. J.; Zhang, R.; Zare, R. N. *J. Phys. Chem.* **1988**, *92*, 5530.
(37) Greene, C. H.; Zare, R. N. *J. Chem. Phys.* **1983**, *78*, 6741.
(38) Altkorn, R.; Zare, R. N. *Annu. Rev. Phys. Chem.* **1984**, *35*, 265.
(39) Demtröder, W. *Laser Spectroscopy*; Springer-Verlag: Berlin, 1988.
(40) Benedict, W. S.; Gailar, N.; Plyler, E. K. *J. Chem. Phys.* **1956**, *24*, 1139.
(41) Toth, R. A.; Brault, J. W. *Appl. Opt.* **1983**, *22*, 908.
(42) Toth, R. A.; Gupta, V. D.; Brault, J. W. *Appl. Opt.* **1982**, *21*, 3337.
(43) Papineau, N.; Flaud, J.-M.; Camy-Peyret, C.; Guelachvili, G. *J. Mol. Spectrosc.* **1981**, *87*, 219.
(44) *CRC Handbook of Chemistry and Physics*, 62nd ed.; Weast, R. C., Ed.; CRC Press: Boca Raton, FL, 1981; pp F-183, F-192.
(45) Herzberg, G. *Molecular Spectra and Molecular Structure, Vol. 1. Spectra of Diatomic Molecules*; Krieger: Malabar, 1989.
(46) Clear, R. D.; Riley, S. J.; Wilson, K. R. *J. Chem. Phys.* **1975**, *63*, 1340.
(47) Reimers, J. R.; Watts, R. O. *Mol. Phys.* **1984**, *52*, 357.
(48) Bowman, J. M. Private communication.
(49) Dieke, G. H.; Crosswhite, H. M. *J. Quant. Spectrosc. Radiat. Transfer* **1962**, *2*, 97.
(50) Clyne, M. A. A.; Coxon, J. A.; Woon Fat, A. R. *J. Mol. Spectrosc.* **1973**, *46*, 146.
(51) Polanyi, J. C. *Acc. Chem. Res.* **1972**, *5*, 161.
(52) Polanyi, J. C.; Wong, W. H. *J. Chem. Phys.* **1969**, *51*, 1439.
(53) Gupta, A.; Perry, D. S.; Zare, R. N. *J. Chem. Phys.* **1980**, *72*, 6250.
(54) Dispert, H. H.; Geis, M. W.; Brooks, P. R. *J. Chem. Phys.* **1979**, *70*, 5317.
(55) Pruett, J. G.; Grabiner, F. R.; Brooks, P. R. *J. Chem. Phys.* **1975**, *63*, 1173; **1974**, *60*, 3335.
(56) Odiorne, T. J.; Brooks, P. R.; Kasper, J. V. V. *J. Chem. Phys.* **1971**, *55*, 1980.
(57) Bronikowski, M. J.; Zare, R. N. *Chem. Phys. Lett.* **1990**, *166*, 5.
(58) Lovejoy, C. M.; Goldfarb, L.; Leone, S. R. *J. Chem. Phys.* **1992**, *96*, 7180.
(59) Coxon, J. A. *Can. J. Phys.* **1980**, *58*, 933.
(60) Rashed, O.; Brown, N. J. *J. Chem. Phys.* **1985**, *82*, 5506.